Engineering Order in the Lattice of LiNbO₃ Crystal Written in Glass by Femtosecond Laser

Collin Barker^{a,*}, Himanshu Jain^b and Volkmar Dierolf^a

^aLehigh University, Department of Physics and Institute for Functional Materials and Devices 18015, PA, USA

ARTICLE INFO

Keywords: fs laser processing single crystal waveguides LiNbO₃ lattice engineering

ABSTRACT

Erbium doped single crystals of lithium niobate were grown within the bulk of 0.075 Er₂O₃ - 37 Li₂O – 37 Nb₂O₅ – 26 SiO₂ glass using a femtosecond pulsed laser. Combined excitation emission spectroscopy was used to show incorporation of erbium into the laser written crystal lattice. Laser power and scanning speed were held constant at optimized values, while bulk sample temperature was systematically varied to study the impact on the crystal growth. Using electron backscatter diffraction to study the transverse cross-sections of grown crystals, control over the lattice rotation rates and crystal size were realized. Unlike changing other parameters, a range of temperatures were found to have substantial impacts on crystal growth, without inhibiting the ability to maintain single crystal formation over long distances.

1. Introduction

Integration of optical elements into a single component is a long-sought goal for higher efficiency and more compact packing with impacts analogous to the development of the microelectronics integrated circuit. As a material, lithium niobate has a wide transparency window around the telecom wavelength band, along with a strong electrooptic response making it a popular candidate material for such optical devices. As such, it is now used in a variety of optical devices, including commercial phase and amplitude modulators[11, 6], polarization controllers[10], nonlinear frequency converters[13], lasers[17], and single photon sources[9].

To use this material in integrated photonics, it is necessary to be able to fabricate it as a waveguide. This has been accomplished via diffusion of titanium[5] and erbium [1, 2] allowing the formation of active waveguides on the surface of its bulk single crystal. Usage of a femtosecond laser to grow LiNbO₃ crystals in glass adds another dimension in which to pack elements in a 3D structure. The waveguiding ability of femtosecond laser written single crystals in glass has been demonstrated in a LaBGeO₅ system [16].

Femtosecond laser crystallization of lithium niobate from glass has been demonstrated by various groups in different glass compositions, [21, 14, 3, 7] but only recently has been shown in the form of large single crystals at the centimeter length scale. Such waveguides sufficiently long for practical applications have been fabricated in a 37 Li₂O -37 Nb₂O₅ - 26 SiO₂ glass composition[18, 19]. An examination of their cross sections by electron backscatter diffraction (EBSD) reveals a continually rotating lattice moving away from the center of the crystal[19]. Lattice rotation in laser written single crystals has also been demonstrated and

*Corresponding author

🙎 cmb719@lehigh.edu (C. Barker) ORCID(s):

analyzed for surface crystallization using a continuous wave laser[12].

In a birefringent material such as LiNbO₃, the special feature of the rotating lattice yields a graded refractive index waveguide, which is expected to confine light more effectively than a usual waveguide. Discovery of a method to engineer such lattice structures would enable control of the confinement of such waveguides and by extension, their optical losses. Additionally, with the introduction of a rare earth dopant, spectral properties may be manipulated by changing the local structural environment of the ion.

Previous works have optimized the growth of single crystals of LiNbO₃ in lithium niobosilicate glass by varying laser power[19], laser repetition rate, laser scanning speed and glass composition[18] to achieve single crystal growth over long distances. A variation of these parameters away from optimized values seems to inhibit the formation of long single crystals and limit the usefulness of such metastructures. In an effort to manipulate the rotating lattice in these laser grown single crystals, in this work we explore the influence of bulk temperature, while assuring single crystal structure without any grain boundaries or segmentation of growth. Furthermore, the capability of engineering crosssectional lattice rotation using this parameter is investigated.

To consider the implications of sample bulk temperature during femtosecond (fs) laser crystallization, it is necessary to understand the nature of crystallization under the laser. Using a high repetition rate fs laser, each pulse is absorbed via multi-photon absorption, yielding localized heat. This heat accumulates through successive pulses and diffuses radially outward, which combined with a linear motion of the sample, produces a complex dynamic temperature profile. The temperature around the focus must be somewhere within the crystal growth range for LiNbO₃. To obtain single crystal growth, all unwanted nucleation must be prevented, while allowing the initial nucleus to form, become a seed and continue to grow into a desired 3D structure. We may consider an arbitrarily defined temperature distribution from the laser.

^bLehigh University, Department of Materials Science and Institute for Functional Materials and Devices 18015, PA, USA

If the bulk temperature is increased without changing the laser power or scanning speed, then the overall temperature distribution would be expected to rise as well, with minimal change to the shape of the profile. Since the glass has a fixed temperature range in which crystal growth can occur, the described control over temperature would affect the volume of the glass in that temperature range. Since the growth rate varies within this temperature range, manipulating the baseline temperature of the profile should enable access to different crystal growth rates as well.

The single crystals grown inside a glass exhibit a rotating lattice because of increase in density upon crystallization and consequently introduction of stresses at the growth front. [12]. Incomplete relaxation of stresses introduces dislocations of a particular kind and curvature to the lattice. Therefore, when manipulating the growth of the crystal by shifting the temperature profile, we can expect that the same will also impact the nature of the rotating lattice. In this work, we characterize the lattice by electron backscatter diffraction (EBSD) and determine the rotation rate of the lattice with the ultimate goal to engineer the single crystal and its lattice for optimal waveguiding properties for applications such as nonlinear optical, rare-earth doped waveguide lasers and rare-earth based quantum memory.

2. Methods

2.1. Glass Making

The procedure for glass making has been described in detail previously for undoped lithium niobosilicate (LNS) glasses [19, 18]. The same procedure is used in this work, with the addition of erbium oxide to the initial mixture. The presence of erbium serves to explore the potential of incorporation into the grown crystal for applications, but is not expected to change the behaviour of the glass during laser crystallization at this concentration. Briefly, powders of Er₂O₃ (99.999%), Li₂CO₃ (99.998%), Nb₂O₅ (99.9985%), and SiO₂ (99.99%) are mixed thoroughly in a ratio that will yield glass of 0.075 $Er_2O_3 - 37 Li_2CO_3 - 37 Nb_2O_5 -$ 26 SiO₂ (Er: LNS-26) composition and then heated up to 1400°C in a platinum crucible. The batch is held for 3 hours at the maximum temperature. Next, the melt is poured onto a stainless-steel plate preheated to 500°C to reduce cracking from thermal shock. The melt is quickly pressed with a second preheated plate, with spacers to control the sample dimensions. The quenched glass is then transferred into a box furnace to anneal at 500°C for 2 hours, before cooling slowly down to room temperature. For laser processing, a piece of the resulting glass is polished to provide an optically smooth surface, minimizing scattering losses at the interface.

2.2. Density Measurement

Densities of bulk glass and crystal samples were obtained using a Mettler Toledo ME balance with the available Density Measurement Kit. The kit was used with deionized water. The reference density of the water at the temperature was obtained from [20].

2.3. Laser Crystallization

A laser beam from Light Conversion PHAROS, operating at 1026nm wavelength with a repetition rate of 200kHz and a pulse width of 175 fs was focused into the bulk of the glass using a Nikon 50x NA 0.6 objective to a depth of 120 μ m below the surface. Using previously optimized parameters for laser power and scanning rate in LNS-26, [18] single crystals were grown for various bulk heating temperatures near the previously used value of 500°C. Any defects at the surface or in the bulk of the glass can cause interruptions in crystal growth. Accordingly, multiple single crystal lines well separated from each other were fabricated for a given temperature; lines that failed to yield a single crystal cross-section due to some defect were not included in further analysis.

2.4. Electron Backscatter Diffraction

To prepare samples for Electron Backscatter Diffraction (EBSD), a low speed diamond saw was used to cut the sample such that the crystal growth direction was along the surface normal. The cut surface was then polished down with the final polishing with colloidal silica (30nm) to minimize topographic distortions inside the scanning electron microscope (SEM). A thin layer of iridium was deposited to prevent charging effects. To acquire ESBD patterns, a Hitachi 4300 SEM was used. The OIM analysis software allowed extraction of indexed Euler angles used throughout this work. Furthermore, the software's local misorientation analysis was used to extract data used to determine the average rotation rates for a given crystal line.

2.5. Combined Excitation Emission Spectroscopy

To study the behaviour of the erbium dopant between the glass and the crystal, combined excitation emission spectroscopy (CEES) is used. First the sample is cooled to 5K, removing the phonon contribution to absorption and emission of the active dopant. Using a custom built microscope, excitation and collection are performed simultaneously. This allows for a small target volume to be probed, which is necessary to study the laser written crystals. A narrow linewidth tunable laser covering the wavelength range of interest is used, taking a spectrum for each step in the tuning range.

3. Results

Before attempting to engineer the crystal lattice, we first tested our ability to fabricate single crystals of lithium niobate since the present Er-doped compostion was never tested previously. To begin, we used the same parameters as for undoped LNS-26 which showed single crystal growth.

Figure 1a shows the SEM image of one laser written single crystal grown within glass at 500°C. The incident laser beam enters from the top of the image, with the growth direction coming out of the plane of the figure. Due to the difference in density between Er:LiNbO₃ and Er:LNS-26, there is visible contrast between the crystal and the surrounding glass. The Inverse Pole Figure (IPF) map in figure 1b is with respect to the surface normal direction. It

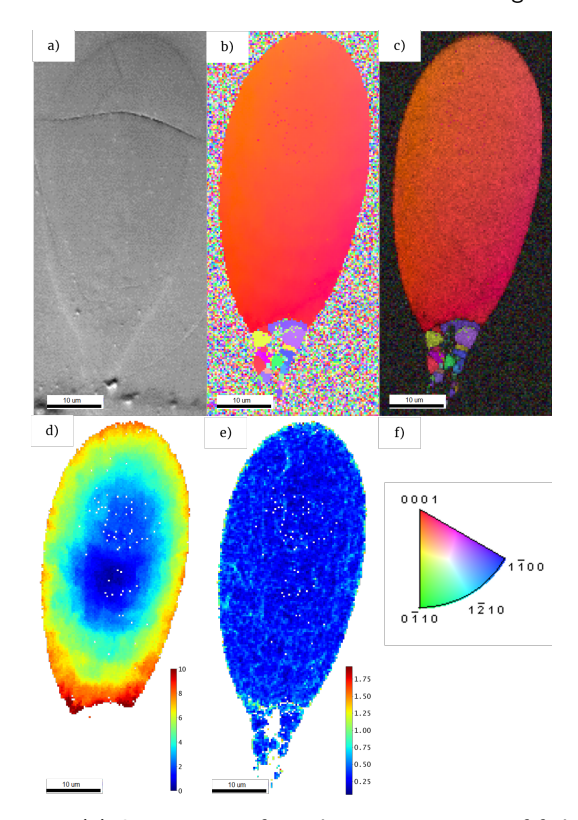


Figure 1: (a) SEM image of 23 plane cross-section of fs laser written single crystal (b) z-axis IPF map of (a) (c) z-axis IPF map with grayscale mask applied based on fit quality (d) misorientation map with respect to crystal center (e) local misorientation map based on nearest neighbor rotations (f) legend for IPF map

shows a single crystal in the middle, with a small region of polycrystalline formation around the base. This is consistent with previous work in LNS, as outside the growth region the temperature is lower and conducive to nucleate new crystals [19]. To remove the glass component from the map, a grayscale based on fit quality is applied yielding figure 1c. In doing so the crystal region can be isolated from the glass, and data from it can be extracted for analysis. As in previous works [19, 18], the single crystal c-axis is nearly parallel to the growth direction. This can be an indicator of the quality of the crystal, as a highly misaligned crystal would mean there was some interruption in the growth, and the crystal had not yet reoriented itself into the preferred direction. We have thus ensured that the change in glass composition has not had a substantial effect on growing lithium niobate single crystals.

3.1. Characterization of Erbium Dopant

While single crystal growth of lithium niobate has now been confirmed, the behaviour of the erbium is of interest. Simply adding a component to the glass composition does not necessarily imply its incorporation into the crystal. Through CEES, the presence of erbium in the crystal can be determined in addition to further exploring the nature of the incorporation into a material. We may therefore determine if the dopant is incorporating into the crystal lattice through comparison with reference samples.

Examination of the CEES maps in fig 2 shows a dramatic change from the erbium in glass to the erbium in a laser written single crystal. Comparison of the laser written crystal to the bulk single crystal indicates that the erbium is in fact in the lattice of the LiNbO₃ grown crystal. Through a closer comparison of the bulk single crystal versus the laser written single crystal, we may see subtle differences in the sharpness of emission and absorption lines. In the bulk crystal individual incorporation sites of erbium within LiNbO₃ is seen as the clusters of very sharp peaks. In our laser written crystals however, these individual sites are washed out as the emission and absorption of erbium are inhomogeneously broadened. This is likely owing to defects in the laser-fabricated crystal[4].

3.2. Varying Sample Baseline Temperature

In previous work, small changes to various parameters including composition, scanning rate, and laser power, inhibited the capability of growing single crystal LiNbO $_3$ over long distances[19]. To prevent cracking from large, localized stresses resulting from the densification of glass upon crystallization, the fs laser processing was performed while the sample was kept at an elevated temperature, but below the glass transition temperature (T_g). Knowing that T_g for this system is 563°C, a range of 450°C to 550°C was selected with 25°C steps. Keeping all other parameters fixed, crystals were grown at each of these bulk sample temperatures. For an initial determination of the impact of these temperature changes, optical micro-graphs were recorded, as shown in figure 3.

For temperatures below 500°C, single crystal formation is disrupted forming segmented lines as shown in Fig. 3. Evidently, crystal growth cannot keep up with the scanning rate as there is insufficient temperature required for continuous growth of single crystals. At 475°C, there are some segments of continuous growth, indicating that this temperature is almost at the threshold. Both lines grown at 500°C and 525°C appear to be single crystal, with the higher temperature line being somewhat wider. This observation makes two points. First, in both cases there is sufficient temperature in the irradiated region to grow the single crystals. Second, in the crystal grown at 525°C, there is a larger growth volume at the necessary temperature. Fig. 3 shows the increase in size of the crystal growth volume as the overall temperature profile is raised. By shifting the overall profile by the temperature change of the bulk sample, different widths meet the growth condition. At 550°C an even larger volume would meet the growth condition, but in the optical image within Fig. 3 it can be seen that the crystal is full of tiny cracks formed by the large interfacial stresses.

For a detailed study of the impact of sample temperature on lattice structure, a more focused range of temperatures was tested in the range of 500°C to 550°C in 5°C steps. Furthermore, to gain a deeper understanding of the crystal structure in these samples EBSD was used. In previous

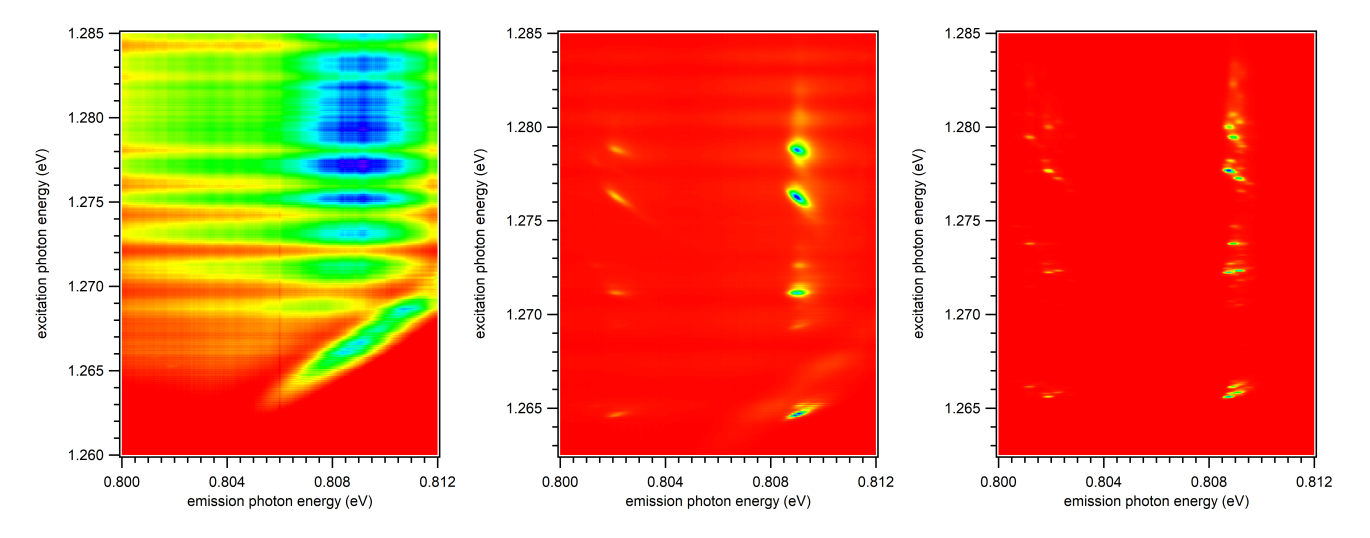


Figure 2: Combined excitation emission spectroscopy maps for the (left) glass, (middle) fs laser written single crystal (right), and bulk stoichiometric 0.19% Er doped LiNbO $_3$ Z-cut crystal. The excitation depicted stimulates the $^4I_{15/2} \rightarrow ^4I_{11/2}$ transition, which under a non-radiative decay leads to emission of $^4I_{13/2} \rightarrow ^4I_{15/2}$

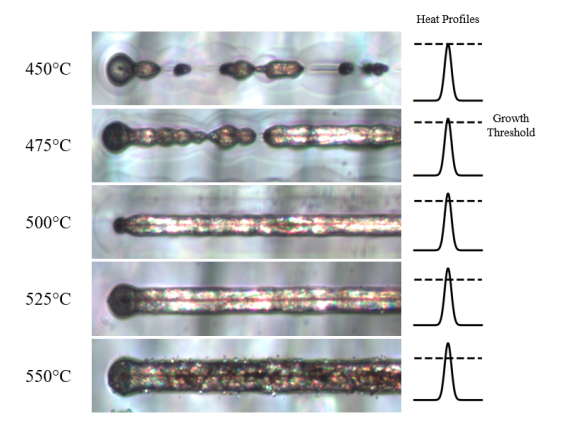


Figure 3: (left) optical micro-graphs of fs laser written crystals over a wide temperature range (right) cross-sectional heat profiles for each line, with fixed crystal growth threshold dashed line.

works, EBSD of a transverse cross-section of a fs laser written crystal showed a fanning out of the crystal lattice, moving away from the center of the crystal [18]. In lithium niobate, this is expected to yield a graded refractive index, and better confined light than a step index crystal in glass [19]. We have now established that the width of these crystals can be optimized via sample bulk temperature. If the lattice rotation rate is consistent, then we would expect a stronger confinement of light due to the graded index. As such, it is necessary to optimize the sample temperature parameter for producing the widest single crystal, and to confirm its quality. Beyond the confirmation of single-crystal growth, we may also consider the stresses present during crystallization and their impact on the crystal structure. Using EBSD more information about the crystal is extracted, including

misorientation with respect to the crystal's center, and local misorientation rates across the cross-section.

Examining crystals grown over the range from 500°C to 550°C, up to 535°C formation of single crystals with the appropriate orientation were verified and mapped by EBSD. Crystals grown at higher temperature were not single crystal and as such maps were not collected from them. In an effort to determine the effect of changing temperature on the rotating lattice of the crystals, two sets of data are extracted from the maps: overall misorientation and local misorientation. Figures 1d,e show these data for one single crystal grown at 500°C. In these two parts of the figure, the misorientation at each position with respect to the crystal's center and the local misorientation rate from nearest neighbors are shown respectively.

By selecting a point in the center of the crystal as a reference orientation, the misorientation angle can be calculated for each pixel and used to generate a map seen in figure 1d. The color scale represents the angle of misorientation of a given pixel to the reference orientation, selected at the center of the crystal. By taking EBSD maps from different temperatures and setting a fixed scale of misorientation across all of them figure 4 is generated. It can be seen that the misorientation at the edge of the crystal is getting higher with increasing temperature. For instance, in the lower temperature cases the edge does not reach 10° , but in the 530° C map the edges are reaching $\sim 20^{\circ}$.

As we observed optically in Fig. 3, the cross-sectional size of the crystal increases with temperature. For a fixed lattice rotation rate, this would lead to a larger total rotation. To quantitatively study crystal size, we use the EBSD of crystal cross-sections.

We determined the crystal cross-sectional area from EBSD data from the size and number of properly indexed pixels in a given map. Figure 5a shows these results for

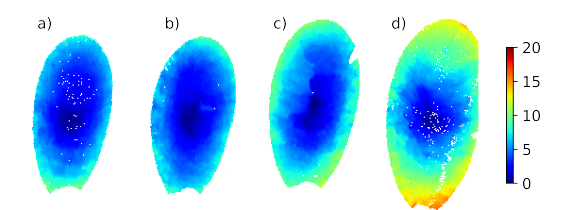


Figure 4: Misorientation maps with respect to center of crystal for fs laser written single crystals grown at (a) 500° C (b) 510° C (c) 520° C (d) 530° C

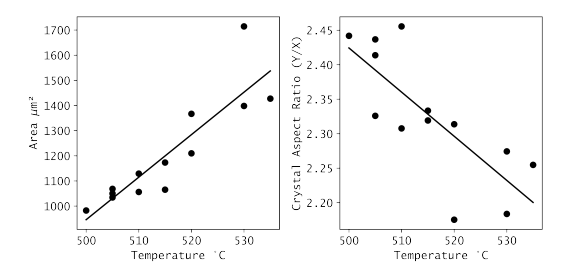


Figure 5: (a) Crystal cross-sectional areas as a function of sample preheat temperature with line of best fit, where areas are determined by counting of pixels after glass removal, multiplied by the step size of the map (b) aspect ratio of indexed crystal after glass removal (height / width) for different sample preheat temperatures with line of best fit

crystal lines fabricated at various temperatures. There is a substantial increase in crystal area with temperature, at about $16.9 \mu m^2/K$. Over the range of $500^{\circ}C$ to $535^{\circ}C$, this corresponds to an average increase in area of 50%. For a fixed lattice rotation rate, the extension of this graded index by that amount is a significant improvement.

In view of the significant changes in the size of crystal cross-sectional area, the question arises about its shape. For a Gaussian beam the aberrations present in the system lead to the characteristic teardrop shape[15]. To determine if the shape of the growth is changing, the aspect ratio is obtained for various crystals. Using the EBSD data, this is determined by cropping away the glass part of the image, and taking the height / width of the indexed region. A plot of this ratio is shown in figure 5b. Here we observe a downtrend with increasing sample temperature. In principle, this effect could be negated using a spatial light modulator, [15] allowing fabrication of a radially symmetric crystal line, which may better confine light.

Up to this point, we have assumed the rate of lattice rotation in the crystal cross-sections to be constant. We have measured the density of a bulk LiNbO $_3$ crystal and of the glass in this work as 4.71 ± 0.02 g/ml and 4.08 ± 0.03 g/ml, respectively. Considering that the modified region is confined deep within the bulk of the glass, the density change during crystallization is a source of stress giving rise to lattice defects, such as dislocations, causing the lattice to rotate as observed. As such, the larger the crystal that forms, the more stress we can expect to be present. By extension, we can also expect the rotation rate to increase. As the

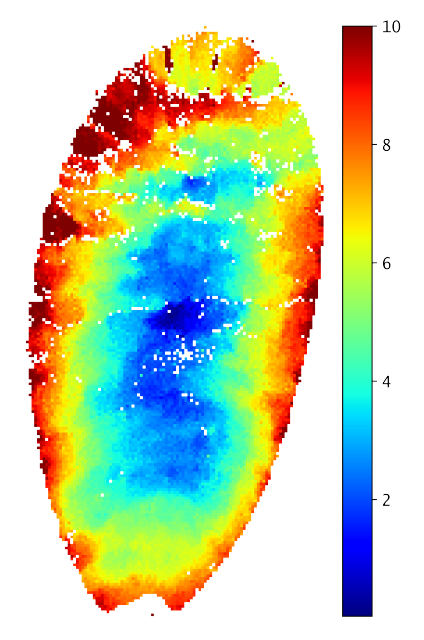


Figure 6: Misorientation map for fs laser written line at 525°C where small angle grain boundaries formed

stress and rotation rate increase, so too must the number density of dislocations that form. Eventually we would then expect that small angle grain boundaries would form as it becomes favorable for the dislocations to stack up[8]. At the upper end of the tested temperature range, we begin to see this phenomenon. As these crystals begin to exhibit small angle grain boundaries, they become clear on examination of misorientation maps such as in figure 6. This observation confirms our expectation of increasing concentration of dislocations, and provides some limitation to our ability to engineer the structure of the crystal in this way, while maintaining the coveted single crystal waveguide.

To probe lattice rotation rates for the successfully formed single crystals, we use the data from figure 1e. By taking all the pixels that indexed to lithium niobate by removing the glass via a fit quality filter, and extracting the rate of misorientation between the nearest neighbors, the map was generated. To compare against other crystals, we take all such values and produce a weighted mean. This procedure does not require selection of a reference orientation unlike the data used for total misorientation maps. In addition, by taking the average of all the values in a map, outliers and small fluctuations within a map can be filtered out. A plot of the average rotation rates against sample temperature is shown in figure 7 along with a histogram of the input data for one map.

Using a linear fit on the average rotation rates versus temperature, we obtain a value of slope as $0.00236^{\circ}/\mu m/K$. The crystals grown at a higher temperature deviate from a linear trend, with a sharp increase in rotation rate with increasing temperature. This is likely due to approaching the transition where small angle grain boundaries become more favorable to form than random dislocations. By examining

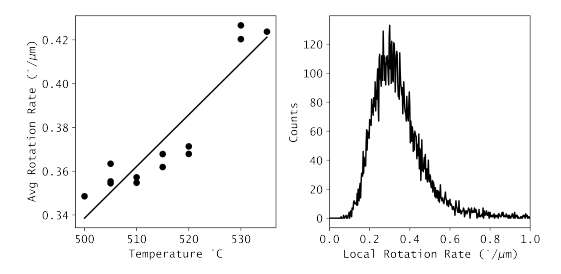


Figure 7: Weighted mean of local rotation rates for each crystal as a function of temperature (left) distribution of local rotation rates from indexed region of single crystal grown at 500°C used to obtain weighted values (right)

a line grown at 525°C, this prediction is confirmed. For the goal of creating the best single crystal waveguide for confining light, it is in this optimized region where the lattice rotation rate is highest, and the crystal size is the largest, both of which are expected to benefit waveguide applications.

Since the shape of the crystal is not axially symmetric, the question arises about the rotation rate for different directions. The method used to study misorientation thus far sacrifices any directionally dependent information in the averages. From the total misorientation maps discussed above, line profiles are acquired to fit rotation along the vertical and horizontal directions independently. By taking a vertical and horizontal line profile through the center of every crystal map, absolute value function fits are used to extract the rotation rate of the lattice for each direction from the slope. This data is presented in figure 8. It is much more sensitive to fluctuations in rotation rate or outliers in the data, since only a small subset of the acquired EBSD data is used. For crystals grown at the lower end of the temperature range good fits are acquired as shown in figure 8a,b, but the crystals grown at the high temperature end begin to deviate as shown in figure 8c,d.

For the horizontal line profiles, there is no clear trend from the acquired data. Whereas there is some variation between crystals, it does not appear that sample bulk temperature is a factor. When examining the vertical line profiles however, we find an increasing trendline. The slope extracted from this least-squares fit is $0.00432^{\circ}/\mu m/K$.

4. Discussion

4.1. Erbium Incorporation

We have demonstrated erbium is present in the crystal, and through comparison with bulk crystal and glass, we determined that the erbium is incorporating into the lithium niobate lattice. The difference between Er in freely grown single crystal and our single crystal laser written under confinement by the surrounding glass matrix is in the broadening of the spectra as seen in Fig. 2. Unfortunately, due to the severity of the spectral broadening, it is not possible to compare individual incorporation sites which are visible in the stoichiometric bulk crystal through the electronic transitions used here. Considering the laser written crystal exhibits

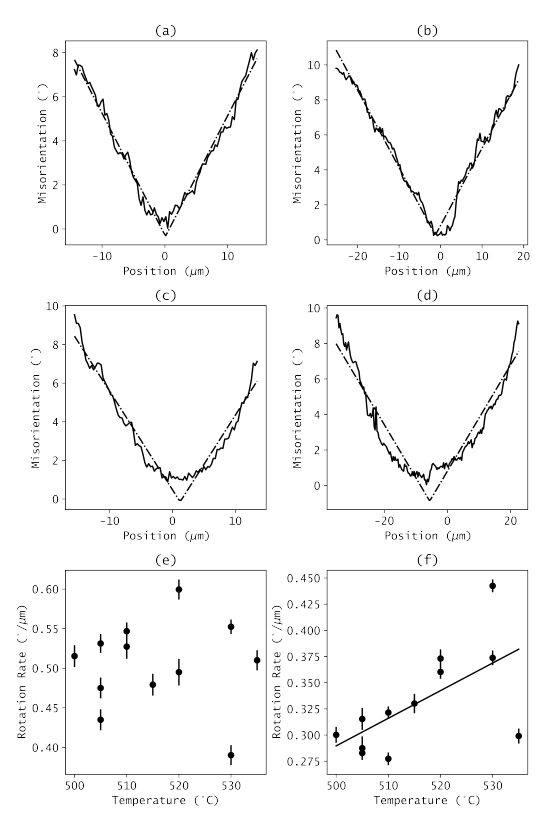


Figure 8: Line profile with absolute value fit of misorientation map of a LiNbO $_3$ single crystal grown at 500°C in the (a) horizontal direction yielding a fit of $0.515^\circ/\mu m$ and the (b) vertical yielding a fit of $0.300^\circ/\mu m$ and for (c, d) a crystal grown at 535°C where fit begins to be less reliable. Slopes for single crystals plotted for the (e) horizontal profiles and (f) vertical profiles, with an increasing trend line fit to data

lattice rotation, made up of a number of randomly placed dislocations, we expect this to be the primary source of the broadening. For applications in which a larger wavelength bandwidth is desirable, as compared to a freely formed bulk single crystal, this would be advantageous. On the other hand, compared to the glass the linewidth is dramatically sharper, which may be of use for applications such as waveguide lasers.

4.2. Useful Temperature Range

The broad range of temperatures used initially determined the viable range in which single crystal growth may be achieved. At too low temperatures, no single crystals could be formed. The cracks seen in fig. 3 on the laser written crystal grown at 550°C suggests that at the elevated temperatures, stresses present during crystallization are higher and the glass can no longer accommodate them. While heating to some extent allows the glass to relieve stress, it is clear that another effect is dominating. As a larger volume of glass is crystallizing, the phase change itself is likely the source of this added stress. Such a damaged crystal would not be useful for wave-guiding due to scattering at the cracks and thus it appears that there is some upper limit to useful temperatures for a given laser power, scanning speed, and

repetition rate. Compared to variation of other processing parameters, fortunately there is a sizeable working range of temperature. In the search for means to fabricate the structure of fs laser fabricated single crystals, this flexibility presents a promising direction.

4.3. Misorientation as a Function of Rate and Size

To explain why the misorientation at the edge of a crystal is changing so dramatically in fig. 4, we consider two effects: changes in crystallized volume, and changes in the rate of lattice rotation in the crystal. If we ignore the aberration in the optical system leading to the teardrop shape of fs laser written crystals, an equation defining the misorientation at the edge of a radially symmetric crystal can be written:

$$\theta = Rate * R_{crystal} \tag{1}$$

where θ is the misorientation at the edge of the crystal, Rate is the lattice rotation rate (which we assume to be constant), and $R_{crystal}$ is the radius of the single crystal. For the purpose of optimizing our crystal metastructure to best confine light within the waveguide, it is desired to maximize θ , which for a birefringent crystal such as LiNbO₃ will yield the largest graded refractive index. Both parameters may be influenced by the sample temperature, and thus should be understood. Since the crystal cross section is not radially symmetric due to aberration, we instead studied the area of a cross section.

Increasing the sample temperature consistently increased the size of grown crystals, up until grain boundaries started forming and single crystal formation was no longer viable. Similarly, the average rotation rate increases with temperature. The dramatic rise in rotation rate above 525°C indicating the formation of small angle grain boundaries would suggest that crystals grown over that temperature may not be viable as waveguides. In the consideration of optimizing crystal growth for the largest refractive index grading, we would aim for the sample temperature to be just below this value.

The line profile analysis of the misorientation maps allowed us to probe anisotropy in the crystal's lattice rotation. We note that the rotation rate extracted for the vertical direction is nearly double the value found for the average rotation rates, but there is no clear trend in the horizontal direction. Averaging the two rotation rates from the line profile analysis yields a value in agreement with the local misorientation rate analysis.

The change observed in the aspect ratio of the crystal as a function of temperature is expected to be due to the shape of the temperature profile. This could suggest that the thermal gradient is higher in the x-direction compared to the y. As such, shifting the overall profile up in temperature brings more volume in the x-direction into the growth range of the crystal as compared to the y-direction. This difference in thermal gradient would most likely be a result of spherical aberration in the focusing of the laser.

5. Summary and conclusions

Our previous work demonstrated the need to use a heating stage to prevent cracking when employing fs laser to fabricate single crystal architecture in glass. Specifically, for LNS-26 composition, at 500°C laser parameters had been optimized to achieve single crystal growth over long distances. Changing the glass composition or the laser processing parameters resulted in inability to grow single crystals over long distances. To engineer the lattice while still being able to grow single crystals, we needed a new processing parameter. The present investigation has demonstrated stage temperature as an effective processing parameter for the fs laser fabrication of 3D single crystal architectures. Relatively small changes in temperature create a large impact on crystal formation through control over crystal size and lattice rotation rates. Furthermore, the increase in lattice rotation rate with temperature illustrates the importance of the stress induced by the transformation of glass into crystal. We have thus established a method for engineering the rotating lattice of fs laser induced growth of LiNbO₃ crystal in LNS glass.

Acknowledgements

This work is funded by NSF DMR-213131 grant under the GOALI program for collaboration between Lehigh University and Corning Incorporated. From Corning we would also like to thank Daniel Nolan for his guidance in this work.

CRediT authorship contribution statement

Collin Barker: Conceptualization, Formal Analysis, Investigation, Data Curation, Writing - Original Draft, Writing - Review and Editing, Visualization. **Himanshu Jain:** Conceptualization, Project Administration, Writing - Review and Editing. **Volkmar Dierolf:** Conceptualization, Project Administration, Writing - Review and Editing.

References

- [1] Becker, C., Oesselke, T., Pandavenes, J., Ricken, R., Rochhausen, K., Schreiber, G., Sohler, W., Suche, H., Wessel, R., Balsamo, S., Montrosset, I., Sciancalepore, D., 2000. Advanced Ti:Er:LiNbO/sub 3/ waveguide lasers. IEEE Journal of Selected Topics in Quantum Electronics 6, 101–113. URL: https://doi.org/10.1109/2944.826878, doi:10.1109/2944.826878. conference Name: IEEE Journal of Selected Topics in Quantum Electronics.
- [2] Brinkmann, R., Sohler, W., Suche, H., 1991. Continuous-wave erbium-diffused LiNbO3 waveguide laser. Electronics Letters 27, 415–417. URL: https://doi.org/10.1049/el:19910263, doi:10.1049/ el:19910263. publisher: IET Digital Library.
- [3] Cao, J., Mazerolles, L., Lancry, M., Brisset, F., Poumellec, B., 2017. Modifications in lithium niobium silicate glass by femtosecond laser direct writing: morphology, crystallization, and nanostructure. JOSA B 34, 160–168. URL: https://doi.org/10.1364/JOSAB.34.000160, doi:10.1364/JOSAB.34.000160. publisher: Optica Publishing Group.
- [4] Dierolf, V., Kutsenko, A., Ostendorf, A., Sandmann, C., 2001. Spectral line broadening mechanism of Er3+ transitions in Er:Ti:LiNbO3 channel waveguides. Applied Physics B 73, 443–448. URL: https://doi.org/10.1007/s003400100692, doi:10.1007/s003400100692.

- [5] Fukuma, M., Noda, J., 1980. Optical properties of titanium-diffused LiNbO₃ strip waveguides and their coupling-to-a-fiber characteristics. Applied Optics 19, 591–597. URL: https://doi.org/10.1364/ A0.19.000591, doi:10.1364/A0.19.000591. publisher: Optica Publishing Group.
- [6] Janner, D., Tulli, D., García-Granda, M., Belmonte, M., Pruneri, V., 2009. Micro-structured integrated electro-optic LiNbO3 modulators. Laser & Photonics Reviews 3, 301–313. URL: https://doi.org/10.1002/lpor.200810073, doi:10.1002/lpor.200810073. _eprint: https://onlinelibrary.wiley.com/doi/pdf/10.1002/lpor.200810073.
- [7] Lotarev, S.V., Lipat'eva, T.O., Lipat'ev, A.S., Naumov, A.S., Shevyakina, D.M., Sigaev, V.N., 2021. Laser Writing of Crystalline Structures in Lithium-Niobium-Germanate Glasses. Glass and Ceramics 77, 409–411. URL: https://doi.org/10.1007/s10717-021-00318-8, doi:10.1007/s10717-021-00318-8.
- [8] Musterman, E.J., Dierolf, V., Jain, H., 2022. Curved lattices of crystals formed in glass. International Journal of Applied Glass Science 13, 402–419. URL: https://onlinelibrary.wiley. com/doi/abs/10.1111/ijag.16574, doi:10.1111/ijag.16574. _eprint: https://onlinelibrary.wiley.com/doi/pdf/10.1111/ijag.16574.
- [9] Namekata, N., Mori, S., Inoue, S., 2007. Single-Photon Source for Telecommunication Wavelengths Using Nondegenerate Photon Pairs from a Periodically Poled LiNbO3 Waveguide. Japanese Journal of Applied Physics 46, 3410. URL: https://doi.org/10.1143/JJAP.46. 3410, doi:10.1143/JJAP.46.3410. publisher: IOP Publishing.
- [10] Noe, R., Koch, B., Mirvoda, V., 2016. LiNbO3-based endless optical polarization control, in: 2016 21st European Conference on Networks and Optical Communications (NOC), IEEE, Lisbon, Portugal. pp. 162–167. URL: https://doi.org/10.1109/NOC.2016.7507006, doi:10. 1109/NOC.2016.7507006.
- [11] Sakamoto, T., Kawanishi, T., Izutsu, M., 2006. Optoelectronic oscillator using a LiNbO3 phase modulator for self-oscillating frequency comb generation. Optics Letters 31, 811–813. URL: https://doi.org/10.1364/OL.31.000811, doi:10.1364/OL.31.000811. publisher: Optica Publishing Group.
- [12] Savytskii, D., Jain, H., Tamura, N., Dierolf, V., 2016. Rotating lattice single crystal architecture on the surface of glass. Scientific Reports 6, 36449. URL: https://www.nature.com/articles/srep36449, doi:10.1038/srep36449. number: 1 Publisher: Nature Publishing Group.
- [13] Schreiber, G., Hofmann, D., Grundkoetter, W., Lee, Y.L., Suche, H., Quiring, V., Ricken, R., Sohler, W., 2001. Nonlinear integrated optical frequency converters with periodically poled Ti:LiNbO3 waveguides, in: Integrated Optics Devices V, SPIE. pp. 144–160. URL: https://doi.org/10.1117/12.426791, doi:10.1117/12.426791.
- [14] Stone, A., 2014. Three-dimensional fabrication of functional single crystal waveguides inside glass by femtosecond laser irradiation. Ph.D.. Lehigh University. United States – Pennsylvania. URL: https://www.proquest.com/docview/1494115738/abstract/ F06E6BF52A4D487DPQ/1. iSBN: 9781303660481.
- [15] Stone, A., Jain, H., Dierolf, V., Sakakura, M., Shimotsuma, Y., Miura, K., Hirao, K., 2013. Multilayer aberration correction for depth-independent three-dimensional crystal growth in glass by femtosecond laser heating. JOSA B 30, 1234–1240. URL: https://opg.optica.org/josab/abstract.cfm?uri=josab-30-5-1234, doi:10.1364/JOSAB.30.001234. publisher: Optica Publishing Group.
- [16] Stone, A., Jain, H., Dierolf, V., Sakakura, M., Shimotsuma, Y., Miura, K., Hirao, K., Lapointe, J., Kashyap, R., 2015. Direct laser-writing of ferroelectric single-crystal waveguide architectures in glass for 3D integrated optics. Scientific Reports 5, 10391. URL: https://doi.org/10.1038/srep10391, doi:10.1038/srep10391. number: 1 Publisher: Nature Publishing Group.
- [17] Suche, H., Baumann, I., Hiller, D., Sohler, W., 1993. Modelocked Er:Ti:LiNbO3-waveguide laser. Electronics Letters 29, 1111–1112. URL: https://doi.org/10.1049/el:19930741, doi:10.1049/el:19930741, publisher: IET Digital Library.
- [18] Veenhuizen, K., Barker, C., Franklin, J., McAnany, S., Aitken, B., Nolan, D., Dierolf, V., Jain, H., 2022. The role of glass composition in the 3D laser fabrication of lithium niobate single crystal in lithium

- niobosilicate glass. Optical Materials 128, 112380. URL: https://doi.org/10.1016/j.optmat.2022.112380, doi:10.1016/j.optmat.2022.112380
- [19] Veenhuizen, K., McAnany, S., Nolan, D., Aitken, B., Dierolf, V., Jain, H., 2017. Fabrication of graded index single crystal in glass. Scientific Reports 7, 44327. URL: https://doi.org/10.1038/srep44327, doi:10.1038/srep44327
- [20] Weast, R., 1972. Handbook of Chemistry and Physics 53rd Edition. Chemical Rubber Pub. URL: https://books.google.com/books?id= aXHKtAEACAAJ.
- [21] Yonesaki, Y., Miura, K., Araki, R., Fujita, K., Hirao, K., 2005. Space-selective precipitation of non-linear optical crystals inside silicate glasses using near-infrared femtosecond laser. Journal of Non-Crystalline Solids 351, 885–892. URL: https://doi.org/10.1016/j.jnoncrysol.2005.01.076, doi:10.1016/j.jnoncrysol.2005.01.076.

Declaration of Interest Statement

Declaration of interests

⊠The authors declare that they have no known competing financial interests or personal relationships
that could have appeared to influence the work reported in this paper.
□The authors declare the following financial interests/personal relationships which may be considered
as potential competing interests: